J Neurophysiol 92: 408–415, 2004.
First published March 10, 2004; 10.1152/jn.01116.2003.

Subthreshold Resonance Explains the Frequency-Dependent Integration of Periodic as Well as Random Stimuli in the Entorhinal Cortex

Susanne Schreiber,[1,*] Irina Erchova,[1,2,*] Uwe Heinemann,[2] and Andreas V. M. Herz[1]
[1]*Institute for Theoretical Biology, Humboldt-Universität zu Berlin, D-10115 Berlin; and* [2]*Johannes Müller Institute for Physiology, Charité, Humboldt-University zu Berlin, D-10117 Berlin, Germany*

Submitted 19 November 2003; accepted in final form 2 March 2004

Schreiber, Susanne, Irina Erchova, Uwe Heinemann, and Andreas V. M. Herz. Subthreshold resonance explains the frequency-dependent integration of periodic as well as random stimuli in the entorhinal cortex. *J Neurophysiol* 92: 408–415, 2004. First published March 10, 2004; 10.1152/jn.01116.2003. Neurons integrate subthreshold inputs in a frequency-dependent manner. For sinusoidal stimuli, response amplitudes thus vary with stimulus frequency. Neurons in entorhinal cortex show two types of such resonance behavior: stellate cells in layer II exhibit a prominent peak in the resonance profile at stimulus frequencies of 5–16 Hz. Pyramidal cells in layer III show only a small impedance peak at low frequencies (1–5 Hz) or a maximum at 0 Hz followed by a monotonic decrease of the impedance. Whether the specific frequency selectivity for periodic stimuli also governs the integration of non-periodic stimuli has been questioned recently. Using frozen-noise stimuli with different distributions of power over frequencies, we provide experimental evidence that the integration of non-periodic subthreshold stimuli is determined by the same subthreshold frequency selectivity as that of periodic stimuli. Differences between the integration of noise stimuli in stellate and pyramidal cells can be fully explained by the resonance properties of each cell type. Response power thus reflects stimulus power in a frequency-selective way. Theoretical predictions based on linear system's theory as well as on conductance-based model neurons support this finding. We also show that the frequency selectivity in the subthreshold range extends to suprathreshold responses in terms of firing rate. Cells in entorhinal cortex are representative examples of cells with resonant or low-pass filter impedance profiles. It is therefore likely that neurons with similar frequency selectivity will process input signals according to the same simple principles.

INTRODUCTION

Various classes of neurons in the central nervous system exhibit a subthreshold resonance of their membrane potential, which means that the amplitude of their voltage responses to sinusoidal currents peaks at a non-zero frequency (Cole 1968; Falk and Fatt 1964; Fishman et al. 1977; Gimbarzevsky et al. 1984; Gutfreund et al. 1995; Hutcheon et al. 1996b; Jansen and Karnup 1994; Leung and Yu 1998; Mauro et al. 1970; Moore and Christensen 1985; Nelson and Lux 1970). There is analytical and experimental evidence that these resonance properties play an important role in tuning neurons to inputs in particular frequency bands (Izhikevich 2001; Haas and White 2002; Richardson et al. 2002) and thus provide a key mechanism to establish a frequency-dependent information flow between cortical areas (Chrobak and Buzsaki 1998; Gloveli et al. 1997).

In the superficial layers of the entorhinal cortex, cells of layers II and III have common cortical input but different hippocampal targets. The cells also respond best to synaptic inputs at different frequency ranges. Layer III pyramidal cells are driven most strongly in the 0- to 5-Hz range, whereas layer II stellate cells are active at frequencies between 5 and 20 Hz (Gloveli et al. 1997; Heinemann et al. 2000). Not surprisingly, stellate cells exhibit a significant subthreshold resonance located in the frequency band of 5–16 Hz. A majority of cells have a peak in the theta band. Pyramidal cells exhibit either a less distinct resonance at low frequencies (1–5 Hz) or no resonance at all (I. Erchova, G. Kreck, U. Heinemann, and A.V.M. Herz, unpublished data).

Resonance properties are usually investigated with sinusoidal inputs or so-called impedance-amplitude profile, where Z denotes the impedance (ZAP) stimuli that consist of sine waves whose frequency changes in time (Gimbarzevsky et al. 1984). It has been questioned, however, whether the findings based on these approaches also extend to more general stimuli, such as randomly fluctuating inputs. One study implies that subthreshold responses to noise stimuli are strongly non-linear and non-resonant and suggests distinctive input-output relations under sub- and suprathreshold conditions (Haas and White 2002).

Because response properties that strongly depend on stimulus characteristics would have far-reaching consequences for our basic understanding of neural dynamics and information processing, we repeated some of the experiments. Extending the original study, we investigated not only layer II stellate cells of the entorhinal cortex (EC) but also EC layer III pyramidal cells. Both cell classes vary strongly in their dynamical characteristics so that generic properties of subthreshold input-output relations can be identified. Our data provide strong evidence that the frequency selectivity for periodic inputs does extend to the non-periodic stimuli used by Haas and White (2002). Contrary to their study, our findings thus support the hypothesis that subthreshold inputs are integrated in an approximately linear fashion. Similarly, we find that responses in the subthreshold and in the spiking regime reflect frequency selectivity rather than overall stimulus power.

METHODS

Experimental methods

SLICE PREPARATION. Horizontal hippocampal slices (400 μm) were prepared from adult Wistar rats (2.5–4 mo, 350–400 g) of both sexes

* S. Schreiber and I. Erchova contributed equally to this study.

Address for reprint requests and other correspondence: S. Schreiber, Institute for Theoretical Biology, Humboldt-Universität zu Berlin, Invalidenstr. 43, 10115 Berlin, Germany (E-mail: s.schreiber@biologie.hu-berlin.de).

The costs of publication of this article were defrayed in part by the payment of page charges. The article must therefore be hereby marked "*advertisement*" in accordance with 18 U.S.C. Section 1734 solely to indicate this fact.

after decapitation under deep ether induced anesthesia in accordance with animal care regulations. Slices were maintained at room temperature in a submerged-style holding chamber until transferred one by one to the recording chamber (36.7°C). Slices were superfused with artificial cerebrospinal fluid (ACSF) containing (in mM) 129 NaCl, 3 KCl, 1.25 NaH_2PO_4*H_2O, 1.8 $MgSO_4$, 1.6 $CaCl_2$*$2H_2O$, 21 $NaHCO_3$, and 10 glucose, pH 7.4; bubbled with carbogen gas 95% O_2-5% CO_2.

RECORDING CONDITIONS. Intracellular recordings in medial entorhinal cortex were done using sharp glass micropipettes (electrode puller P-87, Sutter Instruments), filled with 2 M potassium acetate, 2% biocytin, 75–85 MΩ, in current-clamp mode. Data were amplified (NeroData IR 183), low-pass filtered at 3 kHz, and digitized with an IO-card (DAQ card Al16E4, National Instruments) at a sampling rate of 8 kHz. For stimulus generation and data acquisition, LabView (National Instruments) was used. All recordings were done at 36.7°C, synaptic transmission was blocked by (in μM) 30 6-cyano-7-nitroquinoxalene-2,3-dione (CNQX), 60 2-amino-5-phosphonovaleric acid (APV), 5 bicucculine, and 1 CGP55845A (3-*N*-[1-(s)-(3,4-dichlorophenyl)ethyl]amino-2-(s)-hydroxypropyl-*P*-benzyl-phosphinic acid, a $GABA_B$ blocker, kind gift from Novartis, Basel, Switzerland). All other chemicals were obtained from Sigma-Aldrich, Deisenhofen, Germany.

HISTOLOGY. For staining slices were stored in 4% paraformaldehyde, shortly left in sucrose 30 % and cut at 50 μm. Biocytin was revealed by standard procedure (Horikawa and Armstrong 1988) using fluorescent marker Alexa 466 coupled to avidin (Molecular Probes, Leijden, The Netherlands).

Estimation of impedance curves

Frequency-dependent impedance curves in the subthreshold regime were estimated through the injection of a ZAP current: $I_{ZAP}(t) = I_0 \sin[2\pi f(t)t]$, with $f(t) = f_m t/2T$. Different levels of depolarization were investigated by applying holding currents between −300 and 300 pA. The time-dependent frequency $f(t)$ of the ZAP current was increased from 0 Hz to the maximum frequency f_m = 20 Hz. The overall duration of the ZAP stimulus was 30 s, so that the ZAP current varied slowly enough to obtain a similar precision of the impedance estimate as upon injecting sinusoidal currents as verified in test experiments. Each impedance estimate was based on an average of five recordings of the response to the ZAP current at the same DC level, with $I_0 = 50$ pA. The frequency-dependent impedance was obtained as the Fourier transform of the time-dependent response to a ZAP input divided by the Fourier transform of the ZAP current, $Z(f) = \mathrm{FFT}[V_{ZAP}(t)]/\mathrm{FFT}[I_{ZAP}(t)]$ (Gimbarzevsky et al. 1984; Puil et al. 1986, 1988). The spectral resolution of frequency-resolved impedance measurements is limited by the recording time. In our case, the resolution was 1/30 Hz. In particular, values at "0 Hz" thus refer to the band between 0 and ~0.033 Hz.

In addition, we also calculated the impedance function on the basis of the noise stimuli (see next section) according to the same procedure. Because of the shorter length of noise stimuli, these impedance functions are not as smooth as those obtained from stimulation with ZAP currents.

Impedance curves were fitted with a two-dimensional electrical circuit model (4 fit parameters), designed to account for the resonance properties of neuronal membranes. Electrical circuit models are equivalent to models of linearized voltage-dependent currents, as suggested by Mauro et al. (1970). Interpreted as an electrical circuit (see also Koch 1999), the model consists of two parallel branches. The first branch is characterized by a resistance (R_m) in parallel with a capacitance (C) and mimics the integrative properties of a leaky-integrator. The second branch consists of another resistance (R_L) in series with an inductance (L) and captures the response properties of a delayed rectifying current. Due to its simplicity, this model has been used in various mathematical investigations of subthreshold phenomena (Mauro et al. 1970; Hutcheon and Yarom 2000; Izhikevich 2001; Erchova et al. 2004; Richardson et al. 2002). Experimental impedance curves and the corresponding fits are shown in Fig. 1, *E* and *F*. The fit parameters for the stellate cell were $R_m = 53$ MΩ, $C = 3.0 \times 10^{-4}$ μF, $R_L = 44$ MΩ, $L = 0.9$ H. For the pyramidal cell we obtained $R_m = 52$ MΩ, $C = 3.4 \times 10^{-4}$ μF, $R_L = 1 \times 10^{12}$ MΩ, and $L = 1 \times 10^9$ H. The exact values of R_L and L varied strongly with the fitting. The order of magnitude of their values given here, however, is representative. The very large values for the resistance, R_L, and inductance L indicate that for the pyramidal cells the model effectively reduces to a single RC-branch with a capacitance, C, in parallel with a resistance, R_m. As a consequence, the residual error between data and model fit is not sensitive to modest variations of R_L and L. Interestingly, the RC-branches of the stellate cell and pyramidal cell are characterized by almost identical parameter values.

Noise stimuli

To investigate possible influences of the stimulus statistics on neural response properties, four types of pseudo-random stimuli were generated as in (Haas and White 2002). Gaussian white noise was convolved with a low-pass filter $f(t)$, with $f(t) = e^{-t/\tau}$, for $t > 0$ and zero otherwise. The time constant, τ, determines the cutoff frequency, $f_{cut} = \frac{1}{2\pi\tau}$, of the resulting stimulus. Values of τ used were 80, 20, 10, and 3 ms, leading to cutoff frequencies of ~2, 8, 16, and 53 Hz, respectively. Through the filter operation, the power of the stimulus is distributed unevenly over frequency space. The smaller the cutoff frequency, the more of the total stimulus power is allocated to the lower frequencies. A 2-Hz cutoff stimulus, for example, contains 93% percent of its power in the range <20 Hz (see Fig. 2*A*). The larger the cutoff frequency, the more is power distributed and stimuli become more and more similar to broadband noise. As a consequence, a 53-Hz cutoff stimulus contains only 23% of its power in the frequency band <20 Hz. We refer to the first three types of stimuli as lower-frequency stimuli and the 53-Hz cutoff stimulus type as a broadband stimulus.

All raw stimuli had a duration of 2 s and were normalized to a root-mean-square (RMS) amplitude of 1. The stimuli were then scaled by an amplitude factor between 0 and 250 pA. Depending on each cell, a DC component ranging between −300 and 300 pA was added. For each recording, a total of 40 different realizations of the four stimulus types (10 each) were represented in alternating order.

Linear prediction

For each cell, theoretical predictions for the standard deviation of the voltage response (also specified as RMS) were obtained from the stimulus spectra and the cell's measured impedance function. Assuming linearity, the amplitude spectrum of the voltage response can be predicted as the product of the amplitude spectrum of the input, $\tilde{I}(f)$, and the frequency-dependent impedance function, $\tilde{Z}(f)$. Taking into account that the variance of any time-dependent function equals its integrated power spectrum over positive frequencies, the RMS reads

$$\mathrm{RMS(V)} = \sqrt{\int_0^\infty |\tilde{\mathrm{I}}(f)\tilde{\mathrm{Z}}(f)|^2 \mathrm{d}f}$$

The mean of the input $I(t)$ was subtracted before calculation of the amplitude spectrum $\tilde{I}(f)$.

Conductance-based model neurons

Two types of single-compartment model neurons were implemented in NEURON (Hines 1993). The models were designed to exhibit the subthreshold resonance characteristics of stellate and pyramidal cells, respectively. Care was taken that the overall shape of the impedance functions corresponded to the experimental counter-

parts. The absolute impedance values matched qualitatively. Both types of model neurons contained fast sodium channels (Na), delayed-rectifier potassium channels (K_{dr}), leak channels (leak), and persistent sodium channels (Na_p). In addition, the stellate model neuron contained H channels as well as muscarinic potassium channels (K_m). These two conductances were responsible for the subthreshold resonance in the stellate model neuron. Their influence on subthreshold resonances has been shown experimentally for hippocampal CA1 neurons (Hu et al. 2002). The presence of H currents in stellate cells and their involvement in the generation of subthreshold membrane oscillations has been shown previously (Dickson et al. 2000; Richter et al. 2000). There is also indirect evidence for the presence of K_m currents in these cells because they are affected by retigabine (Hetka et al. 1999), which was recently shown to act on muscarinic potassium channels (Rundfeldt and Netzer 2000; Main et al. 2000). In addition, subunits of muscarinic potassium channels (in the KCNQ family) have been found to be expressed in layer II of the entorhinal cortex (Saganich et al. 2001). Because resonance in stellate cells is observed over a wide range of voltages (from hyperpolarized levels to threshold) and the activation ranges of these two currents cover the hyperpolarized (I_H) as well as the depolarized (I_{Km}) membrane potentials, we chose these currents to model the resonance in stellate cells. The peak conductances of the three ion channel types were $g_{Na} = 24$ mS/cm^2, $g_{Kdr} = 3$ mS/cm^2, and $g_{NaP} = 0.02$ mS/cm^2 in both model neuron types. The other conductances were $g_{leak} = 0.04$ mS/cm^2, $g_{Km} = 0.4$ mS/cm^2, and $g_H = 0.25$ mS/cm^2 (stellate model neuron), and $g_{leak} = 0.07$ mS/cm^2, $g_{Km} = 0$ mS/cm^2, and $g_H = 0$ mS/cm^2 (pyramidal model neuron). The impedance curves for both model neurons measured at rest are shown in Fig. 1, *G* and *H*. For details of the model parameters and kinetics see APPENDIX. Small amounts of white Gaussian current noise were injected in addition to the frozen low-pass-filtered noise currents to simulate intrinsic noise sources (SD of $\sigma_n = 0.01$ nA for the stellate model cell, $\sigma_n = 0.006$ nA for the pyramidal model cell). These values for the SD were chosen to match the noise-induced model voltage fluctuations to the voltage fluctuations observed in experiments. The presence of this additional noise, however, had no significant consequences for the results.

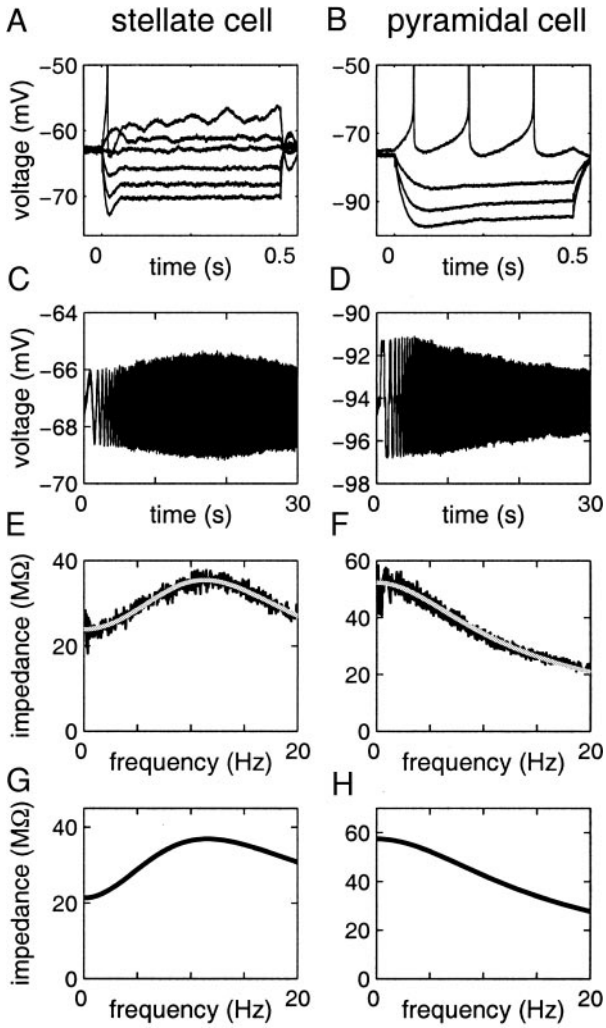

FIG. 1. Characteristic properties of stellate and pyramidal cells (*left* and *right*, respectively) *A* and *B*: voltage responses to DC current injection (*A*: −300, −200, −100, 0, 50, 150 pA; *B*: −300, −200, −100, 50 pA). The stellate cell exhibits membrane potential oscillations at depolarized levels and prominent sag potentials. *C* and *D*: averaged responses to ZAP-current injection (5 repetitions, *C* measured at rest, *D* measured with a DC component of −260 pA). *E* and *F*: experimental impedance functions derived from the response to the ZAP current presented in *C* and *D* (black lines) and the corresponding fits (gray lines) with the electric circuit model described in METHODS, see also (Mauro et al. 1970). Stellate cells showed a pronounced resonance at frequencies ~10 Hz. Pyramidal cells mostly exhibited monotonically decreasing impedance functions; 3 cells also showed a small resonance at low frequencies. *G* and *H*: impedance functions of the 2 conductance-based model cells.

RESULTS

Stable recordings were obtained from 11 entorhinal cortex cells, 6 of which were layer II stellate neurons and 5 were layer III pyramidal neurons. The neurons were morphologically identified based on biocytin staining. We did not distinguish between different subclasses of pyramidal cells for the purpose of this study. Figure 1, *A* and *B*, shows the responses of two representative cells to DC current injections. All stellate cells exhibited a typical sag potential in response to both hyper- and depolarizing currents. For three cells, prominent membrane oscillations in the theta-frequency band were confirmed upon depolarization. No membrane potential oscillations were observed in pyramidal cells. Three pyramidal cells exhibited a sag potential, which had a slower time course than the sag observed in stellate cells. The input impedance, estimated from the response to a current step of either 50 or −50 pA (for cells with very low firing threshold), was 32 ± 11 MΩ for stellate cells, and 72 ± 30 MΩ for pyramidal cells. The resting membrane potential of stellate cells was −65 ± 5 mV, membrane time constants were measured as 6 ± 2 ms. The resting membrane potential of pyramidal neurons was −75 ± 6 mV, their time constants were 21 ± 8 ms. Note that we state mean ± SD throughout the paper.

Subthreshold frequency preference was estimated by injecting a ZAP current. Figure 1, *C* and *D*, shows the average response to five presentations of the ZAP current for the cells characterized in the panels above. The prominent peak of the ZAP response for stellate cells ~17 s translated into a peak in membrane impedance at 11.3 Hz, see Fig. 1*E*. The pyramidal cell, however, exhibited low-pass filter characteristics. The impedance function showed a maximum at 0 Hz and fell off with increasing frequencies. All stellate cells had an impedance peak between 7 and 15 Hz (average across cells: 11 ± 3 Hz) and a pronounced *Q* value (ratio between the impedance at the resonance frequency and the impedance at 0 Hz) between 1.2 and 1.8 (average across cells: 1.5 ± 0.3). Pyramidal cells either did not show a resonance at all or the impedance had a maximum at very low frequencies (between 0 and 5 Hz, with

an average of 3 ± 2 Hz). In addition, the *Q* values of pyramidal cells were low (1.0–1.2, average: 1.1 ± 0.1). For both cell types, the impedances were estimated at a depolarization level that was used for further analysis (i.e. at rest for most cells but also at moderately hyperpolarized or depolarized levels for some cells).

The parameters of the conductance-based model cells were chosen such that their membrane impedance closely matched that of the two representative cells (Fig. 1). For details, see METHODS. The impedances, estimated in the same way as for experiments, are shown in *G* and *H* of Fig. 1.

Integration of noise stimuli in the subthreshold regime

To analyze whether the subthreshold frequency selectivity in response to periodic inputs also influences the integration of non-periodic inputs, we followed Haas and White (2002) and injected four different types of frozen low-pass filtered Gaussian noise stimuli. The four types differed in their cutoff frequency, resulting in broadband type stimuli (f_{cut} = 53 Hz) and stimuli with more power at low frequencies (f_{cut} = 16, 8, and 2 Hz). Figure 2*A* presents the average power spectra of these stimuli. Figure 2*B* presents one example for each stimulus type. Figure 2*C* shows the responses of a representative stellate cell to these stimuli. The raw data demonstrate that the response amplitude is larger for the low-frequency stimuli (f_{cut} = 2, 8, and 16 Hz) and smaller for the broadband stimulus (f_{cut} = 53 Hz), although the RMS values of all injected currents were the same.

Does the response amplitude depend on the shape of the input's power spectrum? If so, can this phenomenon be explained by the frequency selectivity observed for periodic stimuli, as measured by the impedance function? To answer these questions, we quantified the amplitude of the fluctuating responses by their RMS values and compared the different scenarios. Figure 3*A* presents the voltage response RMS values as a function of the input RMS values for the stellate cell described in Fig. 1. The dependence of the response magnitude on the input RMS value is approximately linear. For an input RMS value of 0 all curves approach the baseline noise level (<0.2 mV). For the largest RMS values, the curves bend due to a slight shift of the holding potential during the experiment. Most importantly, however, the response RMS values between the broadband stimulus and each of the lower-frequency stimuli differed strongly. On the other hand, the lower-frequency stimuli were not significantly different from each other. Figure 3*B* shows the average population data of the recorded stellate cells and confirms the differential response power to broadband versus lower-frequency stimuli. For all measured cells, the broadband RMS values were significantly smaller than those of each of the lower-frequency stimuli (confidence level 99% with Student's *t*-test at all amplitudes for all recorded cells, with the exception of the lowest 10 pA amplitude, which was close to the noise level, and with the exception of the 16 and 53 Hz cutoff-frequency responses for the pyramidal cell at 200 pA presented in Fig. 3*E*, where the confidence level was only 80%).

Figure 3*C* depicts the linear theoretical predictions of the response RMS values based on the measured impedance function of the presented stellate cell (see METHODS). The good agreement between prediction and experimental data indicates that responses of stellate cells to periodic inputs as well as to noise-like stimuli can be explained by the subthreshold frequency selectivity. Figure 3*D* presents the corresponding results from the conductance-based model stellate cell. The model results match both, experimental data as well as the theoretical prediction.

Figure 3, *E–H*, shows the same analysis for the pyramidal neuron characterized in Fig. 1. In contrast to the measured stellate cells, the response RMS values differ also among lower-frequency stimuli. As is expected from linear system's theory, taking the measured impedance function into account, the broadband stimulus had significantly lower power than any of the other lower-frequency stimuli. The conductance-based model neuron confirmed this finding.

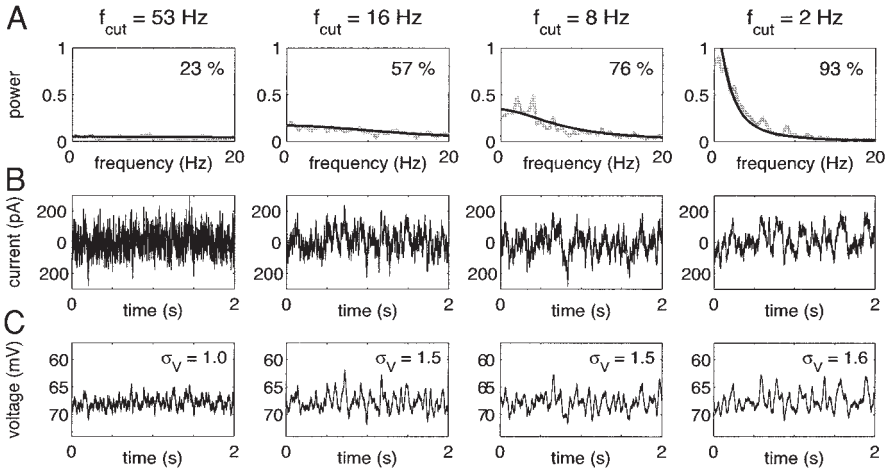

FIG. 2. Stimuli and responses. *A*: actual average power spectra of the 4 stimulus types, which differed in their cutoff frequency, f_{cut}. The black line indicates the idealized theoretical power spectra, the labels in the panel's top right corner denote the percentage of stimulus power that is contained in the frequency band <20 Hz. Lower-frequency stimuli (f_{cut} = 16 Hz and below) have a large percentage of power allocated at frequencies <20 Hz. The stimulus f_{cut} = 53 Hz is more broadband-like and less than ¼ of its power is allocated to frequencies <20 Hz. *B*: examples of individual stimuli. All stimuli have the same standard deviation (RMS = 50 pA). *C*: responses of the stellate cell presented in Fig. 1. The RMS voltage fluctuation is marked in the top right corner. Response amplitudes of the broadband stimulus are significantly lower than those of the lower-frequency stimuli.

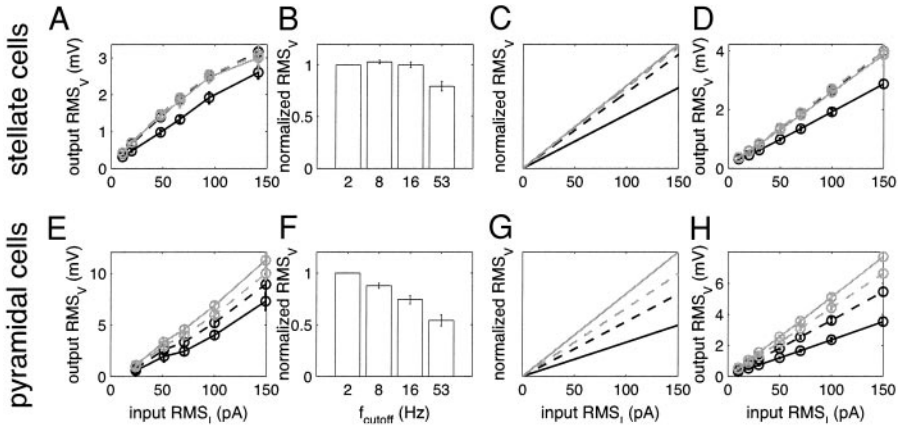

FIG. 3. Frequency selectivity determines response power. *A*: RMS values of the voltage response (mV) as a function of the input RMS (pA) for the stellate cell presented in Fig. 1. Different curves correspond to different types of stimuli, with f_{cut} = 2 Hz (gray solid), f_{cut} = 8 Hz (gray dashed), f_{cut} = 16 Hz (black dashed), and f_{cut} = 53 Hz (black solid). The lowest RMS values are achieved in response to the broadband stimulus. The lower-frequency stimuli yield significantly higher RMS values. In general, the response RMS values increase linearly with stimulus amplitude (or RMS). *B*: relative response RMS values averaged across all stellate cells. The 4 data points for each input RMS value (from curves such as in *A*) were normalized by a factor such that the response RMS values to the f_{cut} = 2 Hz stimulus equal unity. *C*: linear prediction of response RMS values (arbitary units) on the basis of the measured impedance function for the stellate cell in *A.* Despite the simplicity of the linear assumption, theoritical prediction and experimental data match well. *D*: similar results are obtained with the conductance-based stellate model cell. *E–H*: the same set of results for pyramidal cells. The response RMS value decreases monotonically with increasing f_{cut} of the stimulus. Again, frequency selectivity as characterized by the impedance function allows one to predict the response RMS (*G*): the model neuron confirms the observation (*H*). For all presented data, spikes occurring at some of the larger stimulus amplitudes were cut out (10 ms before a spike to 50 ms after the spike). It was checked that the length of these cut out intervals was appropriate to eliminate the effect of spikes.

RMS values reflect only the total amount of power. A more detailed picture is given by the distribution of response magnitude over frequencies, which is depicted in Fig. 4, *A* and *B*, on the basis of the experimental responses. For both cell types, the deviations between the responses to the broadband (f_{cut} = 53 Hz) stimulus and the lower frequency stimulus (as exemplified by the f_{cut} = 8 Hz stimuli) are largest at low frequencies. In addition, the impedance function can also be calculated directly from the responses to noise stimuli. These results are presented in Fig. 4*C* and *D.* Complex-valued impedance functions were obtained for each stimulus and averaged over all stimuli (at fixed input RMS values). This average is justified because there were no significant differences between the impedance functions derived from stimuli with different cutoff frequencies and the impedance fluctuations decrease due to the increased size of the total data set. For the stellate cell, an impedance peak ~10 Hz is visible. For the pyramidal cell, the impedance decreases monotonically. Because the power spectrum of the used broadband noise stimuli is relatively flat (see Fig. 2*A*), the overall shapes of the impedance curves (Fig. 4, *C* and *D*) mirror the amplitude spectrum of voltage responses (Fig. 4, *A* and *B*).

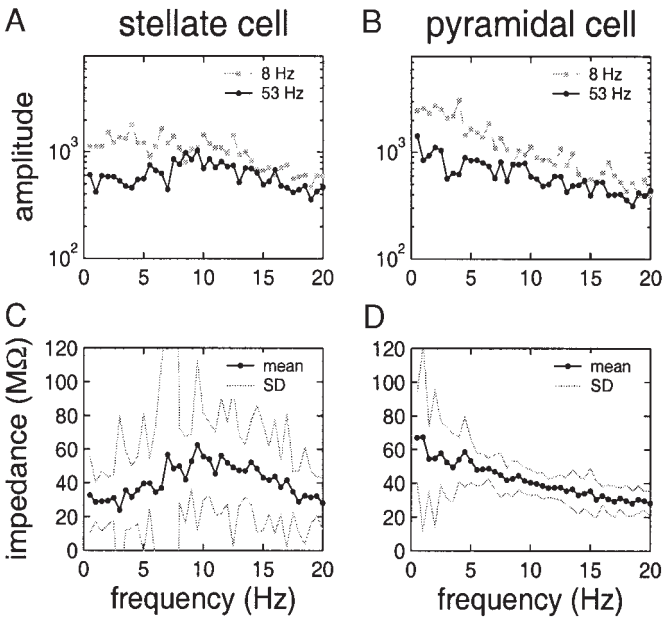

FIG. 4. Impedance can be reconstructed from noise stimuli. *A*: Amplitude spectra of experimental stellate cell responses to broadband (black solid line, f_{cut} = 53 Hz) and lower frequency stimuli (gray dashed line, f_{cut} = 8 Hz), input RMS = 20 pA each. *B*: the same for the pyramidal cell. *C* and *D*: the corresponding impedance functions calculated on the basis of responses to all noise stimuli (at the input RMS = 20 pA). The thin gray lines indicate the SD of the impedance estimate. Clearly, stellate cells show a non-monotonic impedance function with a maximum ~10 Hz, similar to the impedance funtion estimated from ZAP responses (see Fig. 1*E*). For pyramidal cells the impedance function decreases monotonically, as does the impedance estimated from ZAP responses (Fig. 1*F*).

Integration of noise stimuli in the spiking regime

We also examined whether the differential integration of noise stimuli in the subthreshold regime extends to the spiking regime in terms of firing rates. Again, we analyzed responses to the set of noise stimuli injected on top of a subthreshold holding current (or at rest). The amplitudes of the noise stimuli were increased so that spikes were elicited. Figure 5*A* shows the average firing rate of the stellate neuron from Fig. 1 in

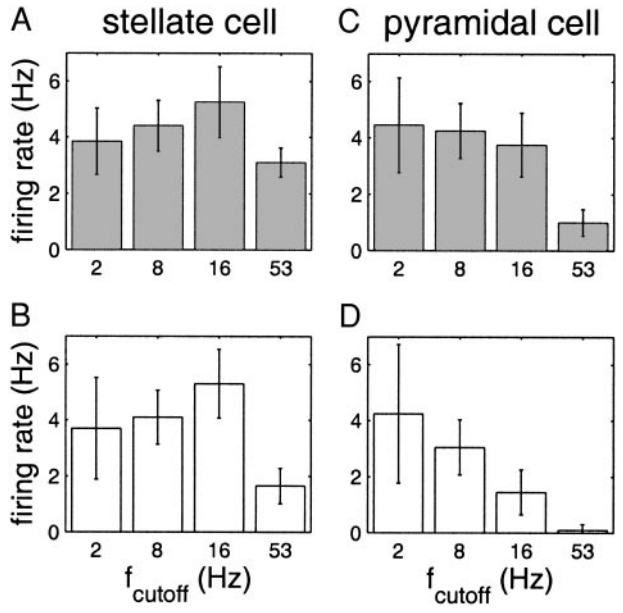

FIG. 5. Subthreshold frequency selectivity influences firing rate. *A*: average firing rate in response to each stimulus type for a stellate cell. Similar to the subthreshold regime the firing rates obtained from responses to the lower-frequency stimuli were larger than that of the broadband type stimuli (input RMS = 200 pA). *B*: the firing rates of the model stellate cell confirm the finding. Stimulus amplitudes (equal for all stimulus types) were adjusted to yield similar firing rates as in the experiments. *C*: for pyramidal cells the firing rate is a monotonic function of the stimulus cutoff frequency, analogous to the subthreshold regime. *D*: qualitatively, the model pyramidal cell shows the same trend. For all panels, the error bars indicate the SD of firing rates within 1 stimulus type.

response to the four noise stimuli (with RMS = 200 pA). Similar to the results in the subthreshold regime, the firing rate evoked by lower-frequency stimuli was higher than that in response to the broadband stimulus (confidence level 99 % with Student's *t*-test for stimuli with 8- and 16-Hz cutoff frequency, 90% for stimuli of 2-Hz cutoff frequency). The result for the model stellate cell showed the exactly same trend. The measured data as well as the model data suggest that the 16-Hz cutoff stimulus elicited the highest firing rate, but the differences between the three lower-frequency stimuli were not significant. An extended analysis with the conductance-based model cell involving a 10-fold higher number of stimuli per stimulus type suggests an equal firing rate for the 8- and 16-Hz cutoff frequency stimuli (firing rate of ~5 Hz), a lower firing rate (~3 Hz) for the f_{cut} = 2-Hz stimulus, and a firing frequency of ~1.5 Hz for the broadband stimulus (data not shown).

For the pyramidal cells, the subthreshold frequency selectivity was also translated into a differential firing rate (Fig. 5*C*). The more stimulus power was allocated to lower frequencies, the higher the firing rate. The *t*-test confirmed a significant difference between the mean firing rate in response to the broadband stimulus and the mean firing rates of the three lower-frequency stimuli (confidence level 99 %). The conductance-based pyramidal model showed a qualitatively similar behavior. Thus the stimuli resulting in larger response amplitudes in the subthreshold regime also cause the cells to fire more strongly. As firing rate data were not available for the cell presented in Fig. 1*B*, data from a different pyramidal cell are shown in Fig. 5*C*. The ratio of firing rates in response to different stimuli types depended on the stimulus amplitude. As expected, there was a regime of smaller amplitudes in both the experiment and model where only the lower-frequency stimuli caused a cell to spike, while no spikes were observed for broadband stimuli of the same RMS value. For larger amplitudes, the broadband stimulus triggered spikes too but did not reach the firing rate of lower-frequency stimuli in the amplitude regime tested.

Additional results about spike timing reliability in response to frozen-noise stimuli can be summarized as follows: in agreement with Fig. 2 of Haas and White (2002), spike jitter depended more strongly on amplitude than on frequency content. Within our limited data set for this specific question (3 cells, 1 amplitude each, 7–10 repetitions per stimulus, 40 different stimuli of 2-s length), the broadband stimulus type did not seem to induce significantly higher jitter than the other stimulus types; although on average more spikes were skipped for broadband stimuli. This may be explained by the lower effective amplitude of broadband stimuli. From our experience, the used stimulus types may not be ideal to test the influence of subthreshold resonance on spike timing reliability.

DISCUSSION

In this study, we have investigated the influence of subthreshold resonance on the cellular integration of incoming signals. Analyzing the responses to low-pass filtered noise stimuli in cells of the entorhinal cortex, we find that the integration of both periodic and non-periodic stimuli is frequency-selective. Experimentally measured subthreshold responses to noise stimuli can be predicted with high accuracy from the frequency-dependent impedance function of a cell and the power spectrum of the stimulus. The integration of periodic and non-periodic inputs is therefore governed by the same mechanism of frequency selectivity and is in full accordance with the response characteristics of a linear system. Consequently, it is not surprising that in pyramidal as well as stellate cells, broadband noise stimuli cause subthreshold voltage responses of significantly less power than stimuli with a higher amount of power allocated at low frequencies. Conductance-based model cells show only minute differences in the integration of signals when compared to experimental observations or linear predictions. This strengthens the view that there is no need for an additional biophysical mechanism that would have a differential effect on the integration of periodic and non-periodic signals.

Subthreshold resonance is shaped by the dynamics of ionic currents (Hutcheon and Yarom 2000), whose activation often depends on the membrane potential. Subthreshold resonances may therefore change with voltage. Resonances shaped by an H current are mainly present at rest and in a hyperpolarized regime. They decrease in size with depolarization because the H current is preferentially activated in the hyperpolarized regime (Hutcheon et al. 1996b). Half-activation voltages in stellate cells were estimated between −77 and −95 mV (Dickson et al. 2000; Richter et al. 2000). In the additional presence of a slow non-inactivating potassium current, such as an K_m current, however, subthreshold resonance can also extend to depolarized values of the membrane potential (Hu et al. 2002). While the currents underlying stellate cell resonance at more depolarized levels of membrane potential have not been iden-

tified yet, it has been found that subthreshold resonance is not constrained to rest or the hyperpolarizing regime. In fact, resonance in stellate cells shows only a small dependence on membrane potential: the impedance values moderately increase toward threshold (I. Erchova, G. Kreck, U. Heinemann, and A.V.M. Herz, unpublished results), as would be expected from voltage-dependent conductances. The change in resonance frequency with voltage is small. Accordingly, we find that the significant difference in response magnitude between broadband stimuli and lower-frequency stimuli is preserved over depolarized and hyperpolarized values of the membrane potential (data not shown). The difference between the stimuli tends to increase toward threshold. Because, overall, resonance in stellate cells does not dramatically change with membrane potential, we do not expect a qualitative dependence of signal integration on membrane potential.

The observed integration of subthreshold signals differs from the findings of Haas and White (2002) in the same experimental system; they do not describe a difference in response magnitude between broadband and lower-frequency stimuli. Comparing the observations in both studies, the responses reported by those authors show a higher level of stimulus-uncorrelated noise. This difference in noise may explain the deviation in the overall RMS voltage response between both studies. Why the studies differ in their observations regarding the response magnitude of broadband and lower-frequency stimuli, however, remains unclear.

We find that the frequency-selectivity for subthreshold stimuli also translates to the spiking regime. When the amplitudes of noise stimuli are increased to elicit spikes, maximum firing rates are obtained for inputs that concentrate power around the resonance frequency. These firing rates, however, are more sensitive to the particular choice of the stimulus set. For model cells, the subthreshold response magnitudes (RMS values) are stable with regard to different stimuli drawn from the same stimulus type, whereas for stimuli with amplitudes large enough to cause spikes, the firing rates depend more strongly on the specific stimuli chosen. The stimulus type eliciting maximum firing rate is either the 16-Hz cutoff stimulus or the 8-Hz cutoff stimulus. This observation goes along with the finding that for the set presented in this paper (Fig. 5), no significant distinction between the 16 and 8-Hz cutoff stimuli could be achieved. Nevertheless, the data indicate that additional non-linearities induced by spiking may influence frequency-selectivity. The effect of subthreshold frequency preference on spiking responses agrees qualitatively with observations made in previous studies, which have shown subthreshold resonance to influence spike timing reliability (Haas and White 2002) and firing-rate modulation (Richardson et al. 2002).

In conclusion, we have shown that the subthreshold frequency selectivity in stellate and pyramidal cells in entorhinal cortex does act equally on different types of stimuli. The output power is fully determined by the power spectrum of the stimulus and the cell's subthreshold frequency preference. The integration of subthreshold signals is approximately linear over a wide range of amplitudes. For spiking responses, the frequency selectivity observed below threshold qualitatively holds; mechanisms such as spike-induced afterhyperpolarization can be expected to slightly modify the frequency selectivity.

Because subthreshold resonances can act as a frequency-dependent amplifier of small-amplitude signals, they are likely to play an important role in the frequency dependent gating of signals to the hippocampus. Our results demonstrate that there is no sudden change in the response characteristics between the subthreshold and the spiking regime. Perhaps surprisingly, responses in both scenarios are well described by simple neuron models.

APPENDIX

The kinetics of all currents were adjusted to 36°C. The value of the capacitance was $C_m = 1\ \mu F/cm^2$. The cell geometry was cylindric with diameter and length measuring 89.2 μm. For the kinetics and parameters of Na, K, Na_p, and leak currents (apart from the peak conductances, which are stated in METHODS), we refer the reader to (Golomb and Amitai 1997). The reversal potentials were $E_{Na} = 55$ mV, $E_K = -90$ mV, $E_{leak} = -80$ mV, $E_H = -43$ mV.

The slow non-inactivating muscarinic potassium current was defined as

$$I_{Km} = g_{Km} n (V - E_K)$$

$$\frac{dn}{dt} = (n_\infty - n)/\tau_n$$

$$n_\infty = \{1 + \exp(-(V - \theta_n)/\sigma_n)\}^{-1}$$

$$\tau_n = 1000\{3.3(\exp((V - \theta_{\tau_n})/\sigma_{1\tau_n}) + \exp(-(V - \theta_{\tau_n}/\sigma_{2\tau_n}))\}^{-1}/T_{adj}$$

$$T_{adj} = 3.0^{(T-22°C)/10°C}$$

where g_{Km} is the peak muscarinic conductance, $E_K = -90$ mV, $\theta_n = -35$ mV, $\sigma_n = 10$ mV, $\theta_{\tau_n} = -35$ mV, $\sigma_{1\tau_n} = 40$ mV, $\sigma_{2\tau_n} = 20$ mV, and $T = 36$°C (for reference, see Yamada et al. 1989; Gutfreund et al. 1995). Technically, values of $\tau_n < 0.001$ were set to 0.001. Exponentials with arguments larger than 50 were set to exp(50).

The H current was defined as

$$I_H = g_H(0.8h_1 + 0.2h_2)(V - E_H)$$

$$\frac{h_1}{dt} = (h_\infty - h_1)/\tau_1$$

$$\frac{h_2}{dt} = (h_\infty - h_2)/\tau_2$$

$$h_\infty = 1/(1 + \exp((V + \theta_H)/7))$$

where g_H is the peak H conductance, $E_H = -43$ mV, $\theta_H = 82$ mV, $\tau_1 = 40$ ms, $\tau_2 = 300$ ms. The equations are based on Spain et al. (1987); see also Bernander et al. (1994) and Hutcheon et al. (1996a).

ACKNOWLEDGMENTS

We thank J. Benda for constructive comments on the manuscript.

Present address of I. Erchova: Unité de Neurosciences Intégratives et Computationnelles, Institut de Neurobiologie Alfred Fessard, CNRS, 91198 Gif-sur-Yvette, France.

GRANTS

This work was supported by grants from the Deutsche Forschungsgemeinschaft (SFB 515 and SFB 618), the German National Merit Foundation, and the Alexander von Humboldt Foundation.

REFERENCES

Bernander O, Koch C, and Douglas R. Amplification and linearization of distal synaptic input to cortical pyramidal cells. *J Neurophysiol* 72: 2743–2753, 1999.

Chrobak J and Buzsaki G. Gamma oscillations in the entorhinal cortex of the freely behaving rat. *J Neurosci* 18: 388–398, 1998.

Cole K. *Membranes, Ions and Impulses.* Berkeley, CA: University of California Press, 1968.

Dickson C, Magistretti J, Shalinsky M, Fransen E, Hasselmo M, and Alonso, A. Properties and role of *I*(h) in the pacing of subthreshold oscillations in entorhinal cortex layer II neurons. *J Neurophysiol* 83: 2562–2579, 2000.

Erchova I, Kreck G, Heinemann U, and Herz AVM. Dynamics of rat entorhinal cortex layer II-III cells: characteristics of membrane potential resonance at rest predict oscillation properties near threshold. *In preparation.* 2004.

Falk G and Fatt P. Linear electrical properties of striated muscle fibers observed with intracellular electrode. *Proc R Soc B Biol Sci* B160: 69–123, 1964.

Fishman H, Poussart D, Moore L, and Siebenga E. K+ conduction description from low-frequency impedance and admittance of squid axon. *J Memb Biol* 32: 255–290, 1977.

Gimbarzevsky B, Miura R, and Puil E. Impedance profiles of peripheral and central neurons. *Can J Physiol Pharmacol* 62: 460–462, 1984.

Gloveli T, Schmitz D, Empson R, and Heinemann U. Frequency-dependent information flow from the entorhinal cortex to the hippocampus. *J Neurophysiol* 78: 3444–3449, 1997.

Golomb D and Amitai Y. Propagating neuronal discharges in neocortical slices: computational and experimental study. *J Neurophysiol* 78: 1199–1211, 1997.

Gutfreund Y, Yarom Y, and Segev I. Subthreshold oscillations and resonant frequency in guinea pig cortical neurons—physiology and modeling. *J Physiol* 483: 621–640, 1995.

Haas JS, and White JA. Frequency selectivity of layer II stellate cells in the medial entorhinal cortex. *J Neurophysiol* 88: 2422–2429, 2002.

Heinemann U, Schmitz D, Eder C, and Gloveli, T. Properties of entorhinal cortex projection cells to the hippocampal formation. *Ann NY Acad Sci* 911: 112–126, 2000.

Hetka R, Rundfeldt C, Heinemann U, and Schmitz D. Retigabine strongly reduces repetitive firing in rat entorhinal cortex. *Eur J Pharmacol* 386: 165–171, 1999.

Hines M. Neuron—a program for simulation of nerve equations. In: *Neural Systems: Analysis and Modeling,* edited by Eeckman F. Norwell, MA: Kluwer, 1993, p. 127–136.

Horikawa K and Armstrong W. A versatile means of intracellular labeling: injection of biocytin and its detection with avidin conjugates. *J Neurosci Methods* 25: 1–11, 1988.

Hu H, Vervaeke K, and Storm J. Two forms of electrical resonance at theta frequencies, generated by M-current, H-current and persistent Na^+ current in rat hippocampal pyramidal cells. *J Physiol* 545: 783–805, 2002.

Hutcheon B, Miura R, and Puil E. Models of subthreshold membrane resonance in neocortical neurons. *J Neurophysiol* 76: 698–714, 1996a.

Hutcheon B, Miura R, and Puil E. Subthreshold membrane resonance in neocortical neurons. *J Neurophysiol* 76: 683–697, 1996b.

Hutcheon B and Yarom Y. Resonance, oscillation and the intrinsic frequency preferences of neurons. *Trends Neurosci* 23: 216–222, 2000.

Izhikevich E. Resonate-and-fire neurons. *Neural Networks* 14: 883–894, 2001.

Jansen H and Karnup S. A spectral analysis of the integration of artificial synaptic potentials in mammalian central neurons. *Brain Res* 666: 9–20, 1994.

Koch C. *Biophysics of Computation: Information Processing in Single Neurons.* New York: Oxford University Press, 1999.

Leung L and Yu H. Theta-frequency resonance in hippocampal CA1 neurons in vitro demonstrated by sinusoidal current injection. *J Neurophysiol* 79: 1592–1596, 1998.

Main M, Cryan J, Dupere J, Cox B, Clare J, and Burbidge S. Modulation of kcnq2/3 potassium channels by the novel anticonvulsant retigabine. *Mol Pharmacol* 58: 253–262, 2000.

Mauro A, Conti F, Dodge F, and Schor R. Subthreshold behavior and phenomenological impedance of squid giant axon. *J Gen Physiol* 55: 497–523, 1970.

Moore L and Christensen B. White noise analysis of cable properties of neuroblastoma cells and lamprey central neurons. *J Neurophysiol* 53: 636–651, 1985.

Nelson P and Lux H. Some electrical measurements of motoneuron parameters. *Biophys J* 10: 55–73, 1970.

Puil E, Gimbarzevsky B, and Miura R. Quantification of membrane properties of trigeminal root ganglion neurons in guinea pig. *J Neurophysiol* 55: 995–1016, 1986.

Puil E, Gimbarzevsky B, and Spigelman I. Primary involvement of K^+ conductance in membrane resonance of trigeminal root ganglion neurons. *J Neurophysiol* 59: 77– 89, 1988.

Richardson M, Brunel N, and Hakim V. From subthreshold to firing-rate resonance. *J Neurophysiol* 91: 000–000, 2004.

Richter H, Heinemann U, and Eder C. Hyperpolarization-activated cation currents in stellate and pyramidal neurons of rat entorhinal cortex. *Neurosci Lett* 281: 33–36, 2000.

Rundfeldt C and Netzer R. The novel anticonvulsant retigabine activates M-currents in chinese hamster ovary-cells transfected with human kdnq2/3 subunits. *Neurosci Lett* 282: 73–76, 2000.

Saganich M, Machado E, and Rudy B. Differential expression of genes encoding subthreshold-operating voltage-gated K^+ channels in brain. *J Neurosci* 21: 4609–4624, 2001.

Spain W, Schwindt P, and Crill W. Anomalous rectification in neurons from cat sensorimotor cortex in vitro. *J Neurophysiol* 57: 1555–1576, 1987.

Yamada Y, Nakazato Y, and Ohga A. Ouabain distinguishes between nicotinic and muscarinic receptor-mediated catecholamine secretions in perfused adrenal-glands of cat. *Br J Pharmacol* 96: 470–479, 1989.